ROYAL SOCIETY
OF CHEMISTRY

PAPER

Check for updates

A polymer donor based on difluoro-quinoxaline with a naphthalimide substituent unit exhibits a low-lying HOMO level for efficient non-fullerene polymer solar cells†

Baitian He, [ID] *[a] Luting Tang,[b] Jinming Zhang,[a] Manjun Xiao,*[b] Guiting Chen [ID] *[a] and Chuanbo Dai[a]

The design and synthesis of polymer donors with a low-lying highest occupied molecular orbital (HOMO) level are crucial for increasing open-circuit voltages (V_{OC}) and achieving high-performance non-fullerene polymer solar cells. Here, we developed two copolymers using non-fluorinated or fluorinated thienyl-conjugated benzodithiophenes as electron donor units, and difluoro-quinoxaline with a naphthalimide substituent (DNB) as the electron acceptor unit. These copolymers, namely PDNB and PDNB-2F, exhibited deep HOMO levels owing to the strong electron-withdrawing ability of the naphthalimide substituent. Density-functional theory calculations demonstrated that the skeletons of the two copolymers featured good coplanarity. Owing to the fluorination, PDNB-2F displayed an increased absorption coefficient and deeper HOMO level than PDNB. Moreover, the blended film based on PDNB-2F:Y6 demonstrated enhanced carrier mobility, decreased bimolecular recombination as well as favorable phase-separation regions. Consequently, the PDNB-2F:Y6-based device yielded a superior power conversion efficiency (PCE) of 12.18%, whereas the device based on PDNB:Y6 showed a comparatively lower PCE of 8.83%. These results indicate that difluoro-quinoxaline with a naphthalimide substituent is a prospective electron-deficient building block to develop donor polymers with low-lying HOMO levels to achieve efficient non-fullerene polymer solar cells.

Introduction

Non-fullerene polymer solar cells (NF-PSCs), which have an active layer comprising a polymer donor and a non-fullerene acceptor, possess unique advantages like flexibility, portability, and solution processability.[1–5] In recent years, the efficiency of NF-PSCs has exceeded 18%, benefiting from significant improvements in non-fullerene acceptors, such as Y6 and its derivatives. These derivatives exhibit robust and extensive absorption profiles in the near-infrared region, thereby increasing the short-circuit current density (J_{SC}) of devices.[6–16] However, the current efficiency of NF-PSCs is still not suitable for commercial applications. To further enhance the performance of NF-PSCs, improving the open-circuit voltages (V_{OC}) of devices is vital. Constructing polymer donors with

lower HOMO energy levels is a viable approach, because the offset between the LUMO of the acceptor and the HOMO of the donor is directly linked to V_{OC}.[17] Several research studies have enhanced the V_{OC} of NF-PSCs by attaching electron-withdrawing substituents, e.g. fluorine atoms, cyano groups, or ester groups, to the electron-deficient building blocks.[18–21]

The difluoro-quinoxaline unit is commonly employed as an electron-deficient central core to construct high-performance donor (D)–acceptor (A) copolymers.[22–26] Extensive studies have focused on altering the difluoro-quinoxaline motif through the attachment of electron-withdrawing substituents to adjust the energy levels of copolymers. For example, the Zou group,[27,28] and the Li group[14,29] have developed several difluoro-quinoxaline-based copolymers with alkoxy-substituted fluorobenzene or alkyl-substituted fluorothiophene side chains to fine-tuning the energy levels of copolymers. PCEs of 9–18% could be achieved through the use of ITIC or Y6 as an acceptor. Moreover, numerous researchers have reported that naphthalene imide is an exceptional electron-withdrawing unit often used to construct n-type semiconducting materials. Such as, Yan et al. developed the naphthalene diimide-based copolymer N2200,[30] and using N2200 as polymer acceptor to construct all polymer solar cells could achieve PCE over 11%.[31] Jenekhe and co-workers reported

[a]School of Chemistry and Environment, Guangdong Rare Earth Photofunctional Materials Engineering Technology Research Center, Jiaying University, Meizhou 514015, P. R. China. E-mail: baitian-he@foxmail.com; cgt_jy@126.com

[b]College of Chemistry, Key Lab of Environment-Friendly Chemistry and Application (Ministry of Education), Xiangtan University, Xiangtan 411105, P. R. China. E-mail: xiaomj7425@xtu.edu.cn

on tetraazabenzodifluoranthene diimides-based molecular BFIs as n-type organic semiconductors,[32,33] Park groups reported dicyanodistyrylbenzene-based compound NIDCS as small molecular acceptor for organic solar cells[34] and Wu groups designed naphthalenothiophene imide-based copolymer PNTB as polymer donor for organic solar cells with an efficiency of 16.72%.[35,36] These materials exhibited HOMO energy levels that were relatively low. Additionally, the naphthalene imide moiety could enhance the planarity of molecular backbone, thus improving carrier mobility. Considering the above, the use of the naphthalene imide unit as an electron-withdrawing substituent to develop difluoro-quinoxaline-based polymer donors has the capability to significantly decrease the HOMO value.

In this work, we report two copolymers, namely PDNB and PDNB-2F, which are derived from non-fluorinated or fluorinated thienyl-conjugated benzodithiophenes (BDT and BDT-2F) as the electron-donating component, and difluoro-quinoxaline with a naphthalimide substituent as the electron-accepting component (Fig. 1a). The difluoro-quinoxaline with a naphthalimide substituent not only could downshift copolymer HOMO level, but also the rigid and good planarity backbone could promote intra-molecular charge transfer. Besides, the N-alkyl side chain could guarantee good solubility of copolymers. The E_{HOMO} for PDNB and PDNB-2F were −5.49 and −5.60 eV, respectively, due to the strong electron-withdrawing ability of the naphthalimide substituent. DFT calculation results showed that both copolymers possessed a well-defined coplanar structure. Owing to fluorination, PDNB-2F displayed a greater absorption coefficient compared to PDNB. When small-molecular acceptor Y6 was used, PDNB-2F:Y6-based device yielded a maximum PCE of 12.18%, while PDNB:Y6-based device displayed a PCE of 8.83%.

The enhanced in PCE is related to the blended film based on PDNB-2F:Y6 displayed enhanced carrier mobilities and appropriate morphology. This work highlights the significant potential of using difluoro-quinoxaline with a naphthalimide substituent as an electron-deficient motif for constructing efficient polymer donors in NF-PSCs.

Results and discussion

Polymer synthesis route

Fig. 2 illustrated the synthesis pathway for PDNB and PDNB-2F, and comprehensive synthetic procedures are provided in the ESI.† Compounds M6 and M7 or M8 were used to synthesize the copolymers PDNB and PDNB-2F, respectively, by using Stille coupling reaction. The number-average molecular weights (M_n) were calculated as 35.99 and 39.31 kDa with a polydispersity indices of 2.43 and 2.73 for PDNB and PDNB-2F, respectively. Thermogravimetric analysis (Fig. S9, ESI†) showed the onset decomposition temperatures at 5% weight loss were 461.7 and 463.2 °C for PDNB and PDNB-2F, respectively, indicating that the resultant copolymers displayed exceptional thermal stability.

Photophysical and electrochemical properties

The absorption coefficient for PDNB and PDNB-2F in chloroform (CF) solution (concentration: 1×10^{-5} M) and as neat films are presents in Fig. 3, and the corresponding values are provided in Table 1. In solution, both PDNB and PDNB-2F exhibited wide absorption spectra. The π–π* transitions were associated with the short wavelength range, whereas the
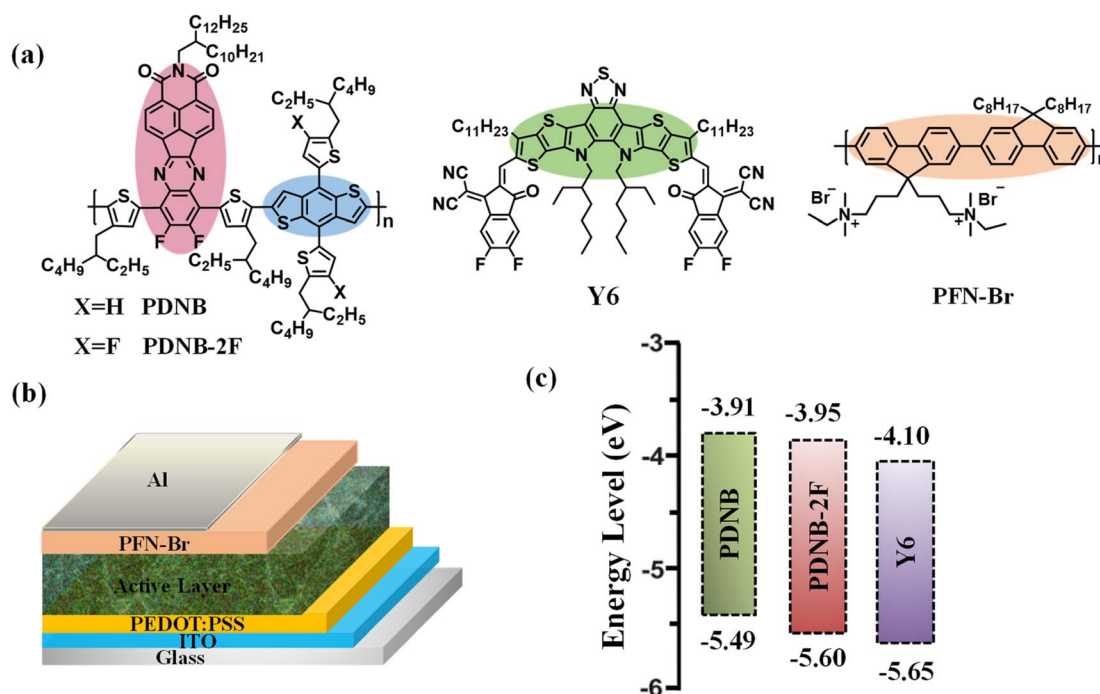

Fig. 1 (a) Chemical structure for PDNB, PDNB-2F, Y6 and PFN-Br. (b) Device architecture of NF-PSCs. (c) Energy-level diagram for PDNB, PDNB-2F, and Y6.
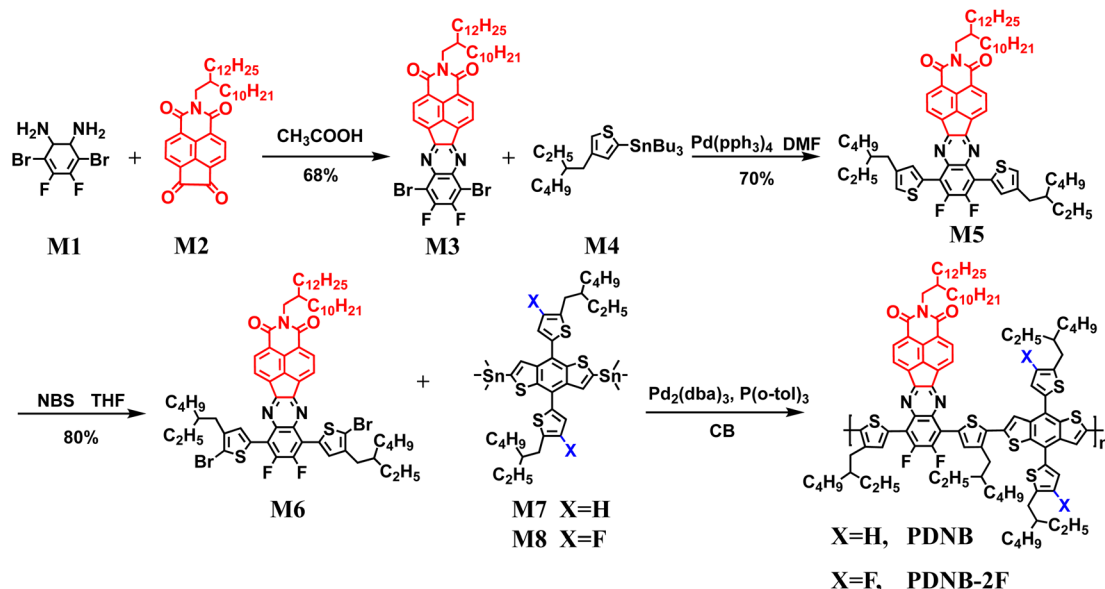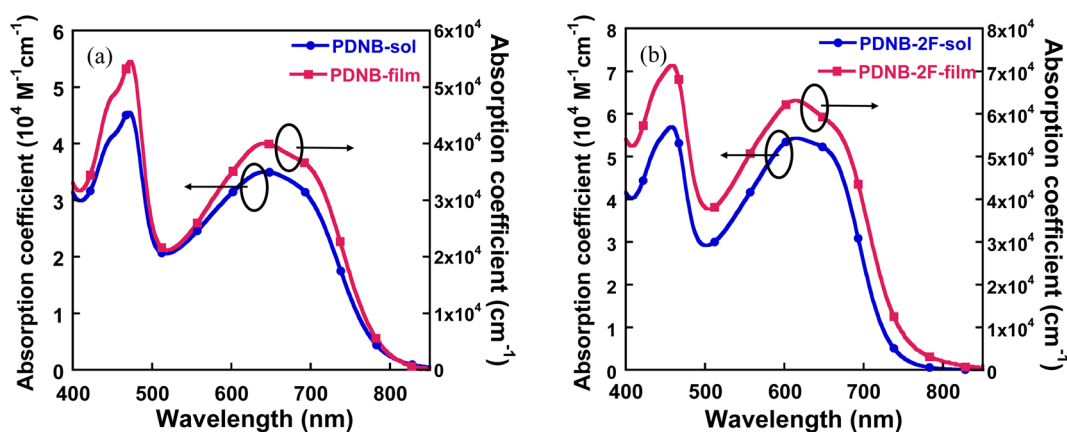
Fig. 2 Synthetic route for PDNB and PDNB-2F.

Fig. 3 Absorption coefficient spectra of solution and as neat films of (a) PDNB and (b) PDNB-2F.

Table 1 Photophysical and electronic properties of PDNB and PDNB-2F

Copolymers	M_n (kDa)	PDI	λ_{onset}^{sol} (nm)	λ_{onset}^{film} (nm)	$E_g^{opt a}$ (eV)	HOMO[b] (eV)	LUMO (eV)
PDNB	35.99	2.43	775	785	1.58	−5.49	−3.91
PDNB-2F	39.31	2.71	733	753	1.65	−5.60	−3.95

[a] Estimated from copolymers film: $E_g^{opt} = 1240/\lambda_{onset}$. [b] Determined using cyclic voltammetry.

intramolecular charge-transfer characteristics corresponded to the absorption peak at longer wavelengths.[19] The maximum absorption coefficients in the solution were 4.52×10^4 and 5.69×10^4 M^{-1} cm^{-1} for PDNB and PDNB-2F, respectively. In the solid state, the absorption spectra exhibited a slight redshift, with absorption onsets at 785 and 753 nm for PDNB and PDNB-2F, respectively. Additionally, the maximum absorption coefficients were 5.7×10^4 and 7.2×10^4 cm^{-1} for PDNB and PDNB-2F, respectively. These results suggest that fluorination

enhanced the extinction coefficient of copolymer, which is favourable for improving the J_{SC} in corresponding device.

The HOMO energy levels of PDNB and PDNB-2F were determine *via* the electrochemical cyclic voltammetry method. The onset oxidation (E_{ox}) potentials for PDNB and PDNB-2F were 1.18 and 1.07 V, respectively (Fig. S10, ESI†). Consequently, the E_{HOMO} were calculated as −5.49 and −5.60 eV for PDNB and PDNB-2F, respectively. The E_{LUMO} were determined using equation $E_{LUMO} = E_{HOMO} + E_g^{opt}$. Compared with PDNB,

PDNB-2F exhibited downshifted HOMO levels, thereby leading to higher V_{OC} in resulting NF-PSCs.

Theoretical calculations

DFT calculations were performed at the B3LYP level using the 6-31G* basis set to analyze the electronic properties and determine the optimal geometries of the copolymers.[18] Fig. 4 shows that the copolymers exhibited well-distributed HOMO surfaces on whole conjugated chain, while LUMO surfaces are primarily concentrated on DNB unit (Fig. 4), suggesting that notable charge transport occurred between the acceptor and donor motifs. Moreover, the PDNB and PDNB-2F displayed dihedral angles of 0.42° and 1.71° between DNB and thiophene unit, respectively, and the dihedral angles of 3.04° and 2.48° occurred between thiophene and BDT units for PDNB and PDNB-2F

(Fig. S11, ESI†), indicating that the fluorine atoms on BDT unit did not considerably affect planarity of the resulting copolymer skeleton.

Photovoltaic properties

NF-PSCs were fabricated with a conventional geometry of ITO/PEDOT:PSS/copolymer:Y6/PFN-Br/Al to evaluate the photovoltaic performance of PDNB and PDNB-2F. The cathode interlayer using poly[(9,9-bis(3-((N,N-dimethyl)-N-ethylammonium)propyl)-2,7-fluorene)-alt-2,7-(9,9-dioctylfluorene)]dibromide (PFN-Br) due to its ability to form an interfacial dipole that promotes electron collection.[37,38] The power conversion efficiency of NF-PSCs were systematically optimized using PDNB:Y6 in terms of spin coating speed, D-to-A weight ratios, annealing temperatures, and additive ratio (Fig. S12–S17 and
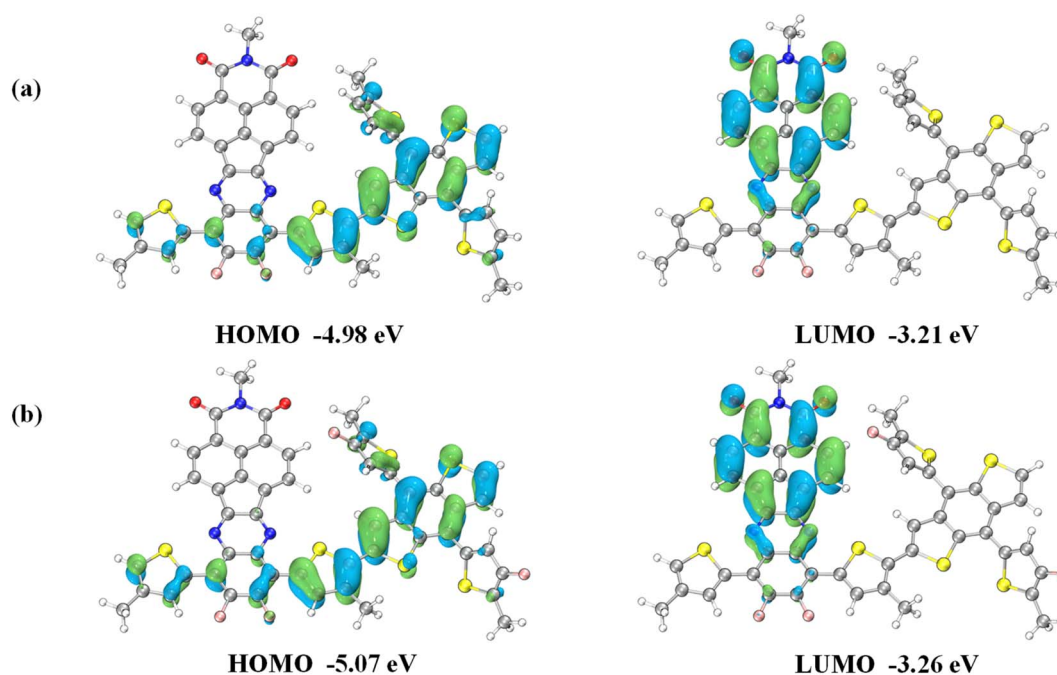

HOMO −4.98 eV   LUMO −3.21 eV

HOMO −5.07 eV   LUMO −3.26 eV

Fig. 4 Energy levels of optimized geometries of one repeating unit for (a) PDNB and (b) PDNB-2F.
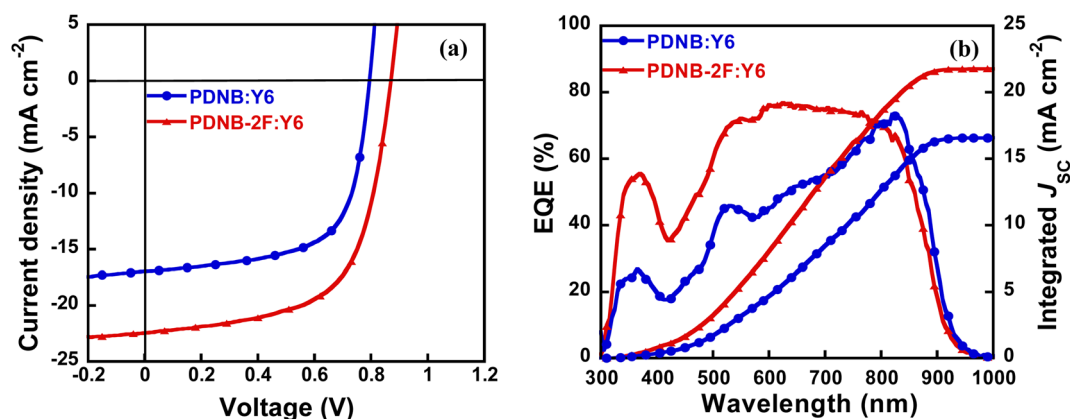

Fig. 5 *J–V* characteristics (a) and EQE spectra (b) for copolymer:Y6-based NF-PSCs.
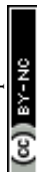
Table 2 Photovoltaic parameters for PDNB:Y6 and PDNB-2F:Y6-based devices

Blend films	V_{OC} (V)	J_{SC} (mA cm^{-2})	$J_{SC\ (Calc)}$[b] (mA cm^{-2})	FF (%)	PCE[a] (%) (max)
PDNB:Y6	0.795	16.97	16.57	65.47	8.83
PDNB-2F:Y6	0.870	22.45	21.78	62.37	12.18

[a] PCE was obtained from 10 separate NF-PSCs. [b] Integrated J_{SC} values from EQE spectra.

Tables S1–S4, ESI†). The optimal copolymer-to-Y6 ratio was determined as 1 : 1.2 (w/w). The spin coating speed of blended film was 1200 rpm. The blended films were fabricated using a CF solution in the absence of additive, then thermal annealing at 100 °C. Fig. 5a and Table 2 presents the J–V curves and parameters of photovoltaic devices. PDNB:Y6-based device exhibited a moderate PCE of 8.83%, J_{SC} of 16.97 mA cm^{-2}, V_{OC} of 0.795 V, while PDNB-2F:Y6-based device yielded a remarkably enhanced PCE of 12.18%, J_{SC} of 22.45 mA cm^{-2}, V_{OC} of 0.870 V. The enhanced V_{OC} and J_{SC} of PDNB-2F:Y6-based device are attributable to the deeper HOMO level and higher absorption coefficient of copolymer PDNB-2F.

The external quantum efficiency (EQE) spectra of NF-PSCs are shown in Fig. 5b. PDNB:Y6 and PDNB-2F:Y6-based NF-PSCs displayed photo-responses from 300 to 900 nm. PDNB-2F:Y6-based NF-PSCs exhibited stronger EQE responses than the device based on PDNB:Y6 in the range of 300–800 nm, consistent with the greater J_{SC} of the former. Moreover, the integrated J_{SC} values were 16.57 and 21.78 mA cm^{-2} for PDNB:Y6 and PDNB-2F:Y6-based devices, respectively, which aligns with the values achieved from J–V curves.

Charge generation, transport, and recombination

To clarify the distinctions performance of PDNB:Y6 and PDNB-2F:Y6-based devices, the charge dissociation and collection properties of these two copolymer-based devices were estimated using photocurrent density J_{ph} ($J_{ph} = J_L - J_D$) and effective voltage V_{eff} ($V_{eff} = V_0 - V_{bias}$) curves, where V_0 is the voltage at J_{ph} is zero and V_{bias} is the applied bias, J_D and J_L denote dark and light current densities, respectively.[39] Fig. 6 shows that J_{ph} reaches
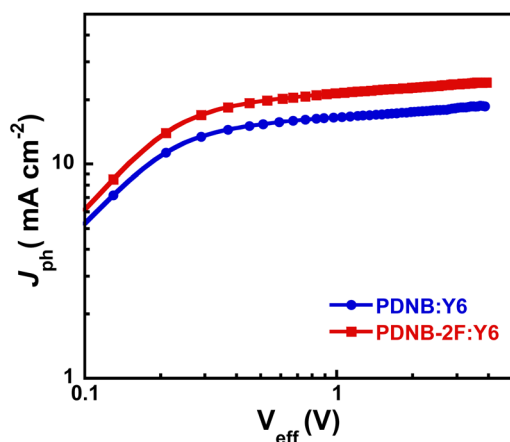
saturation current (J_{sat}) at a V_{eff} value greater than 2 V, indicating that the photogenerated excitons separated into free charges. The charge seperation probability $P(E,T)$ can be calculated by the ratio of J_{ph}/J_{sat} (Table S7†).[40] The $P(E,T)$ values were 93.5% for PDNB:Y6-based device and 94.4% for PDNB-2F:Y6-based device under J_{SC} conditions, implying the device based on PDNB-2F:Y6 possessed highly efficient excitons separation and charge extraction properties, consistent well with its higher J_{SC}.

The carrier mobilities of blend films were measured by using the SCLC method to study the charge transport properties of the devices (Fig. S18, ESI†).[41] The detailed values are presented in Table 3. The hole mobility (μ_h)/electron mobility (μ_e) values of PDNB:Y6- and PDNB-2F:Y6-based blended films were 1.18 × 10^{-4}/2.23 × 10^{-4} and 1.52 × 10^{-4}/2.47 × 10^{-4} cm^2 V^{-1} s^{-1}, respectively. Thus, PDNB-2F:Y6-based blended film displayed greater and a better μ_e/μ_h balance than PDNB:Y6-based blended film, leading to the higher J_{SC} in PDNB-2F:Y6-based device. Moreover, a photoluminescence quenching experiment was carried out to investigate exciton dissociation and charge transfer in blend films (Fig. S19, ESI†). The quenching of the photoluminescence intensity of PDNB-2F:Y6-based blended film is more pronounced than that of PDNB:Y6-based blended film, indicating more efficient exciton dissociation and charge transfer in PDNB-2F:Y6-based blend film. These findings are consistent with the enhanced PCE of PDNB-2F:Y6-based device.

Furthermore, to evaluate the bimolecular recombination behaviour of NF-PSCs, the dependence of J_{SC} on light intensities (P_{light}) was conducted (Fig. 7a). The relationship between P_{light} and J_{SC} can be expressed as $J_{SC} \propto (P_{light})^S$. In general, the devices exhibited minimal bimolecular recombination when the S value approaches 1.[42] The S values were 0.988 and 0.991 for device based on PDNB:Y6 and PDNB-2F:Y6, respectively. The PDNB-2F-based device exhibited a higher S value, indicating bimolecular recombination could be effectively suppressed in its device, which corresponds to the improved J_{SC}. Additionally, Fig. 7b illustrates the P_{light} versus V_{OC} curves to study recombination processes of NF-PSCs. The slopes derived from the curves of PDNB:Y6 and PDNB-2F:Y6-based NF-PSCs were 1.25 and 1.01 kT/q, respectively, indicating reduced charge recombination in the PDNB-2F:Y6-based device.[43]

Fig. 6 J_{ph}–V_{eff} curves of PDNB:Y6 and PDNB-2F:Y6-based devices.

Table 3 Carrier mobilities of PDNB:Y6 and PDNB-2F:Y6-based devices

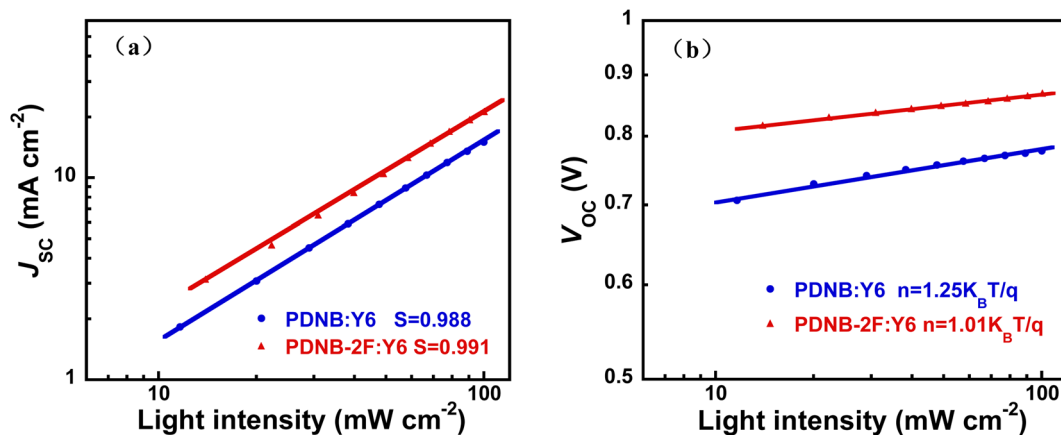| Blended films	μ_h (cm^2 V^{-1} s^{-1})	μ_e (cm^2 V^{-1} s^{-1})	μ_e/μ_h
PDNB:Y6	1.18 × 10^{-4}	2.23 × 10^{-4}	1.89
PDNB-2F:Y6	1.52 × 10^{-4}	2.47 × 10^{-4}	1.62

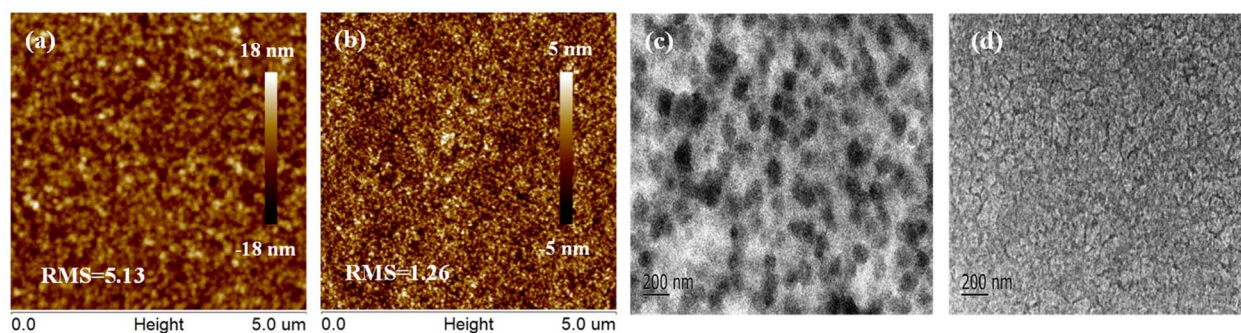**Fig. 7** P_{light} *versus* J_{SC} (a) and V_{OC} (b) of PDNB:Y6 and PDNB-2F:Y6-based devices.

Fig. 8 AFM height images of PDNB:Y6-based (a) and PDNB-2F:Y6-based (b). TEM images of PDNB:Y6-based (c) and PDNB-2F:Y6-based (d) of the optimal blended films.

Morphology investigation

To analyze the morphologies of the blended films, atomic force microscopy (AFM) and transmission electron microscopy (TEM) measurements were performed. Fig. 8a and b illustrate PDNB:Y6 and PDNB-2F:Y6 displayed discernible surface morphologies, characterized by root mean square values of 5.13 and 1.26 nm, respectively. Compared to PDNB:Y6-based blended film, PDNB-2F:Y6-based blended film exhibited a sleek and uniform surface, which facilitated charge separation and collection, ultimately leading to a higher J_{SC}.[44] Moreover, we conducted TEM measurements to study the morphologies of the optimal active layers. PDNB:Y6-based blended film exhibited large phase domains, whereas PDNB-2F:Y6-based blended film displayed a more suitable nanoscale phase separation morphology (Fig. 8c and d). This favorable morphology contributed to efficient excitons separation and charge transportation, thereby enhanced the J_{SC} in PDNB-2F:Y6-based NF-PSCs.

Conclusion

We reported two copolymers, namely PDNB and PDNB-2F, based on BDT or BDT-2F, as the donor motif and difluoro-quinoxaline with naphthalimide substituent as the acceptor motif. The two copolymers exhibited downshifted HOMO energy levels. PDNB-2F exhibited a higher absorption coefficient than PDNB. NF-PSCs based on PDNB-2F:Y6 gave the maximum PCE of 12.18%, V_{OC} of 0.87 V, whereas the device based on PDNB:Y6 showed a PCE of only 8.83%. The enhanced performance of was due to weaker bimolecular recombination, enhanced carrier mobilities, and favorable morphology in the PDNB-2F:Y6-based blended film. The results demonstrate that using difluoro-quinoxaline with a naphthalimide substituent as an electron-deficient unit is a promising approach to fabricate electron donors with downshifted HOMO levels for efficient NF-PSCs.

Author contributions

Baitian He: writing – original draft, project administration, supervision. Luting Tang: data curation, methodology. Jinming Zhang: synthesized the polymers, formal analysis. Manjun Xiao: investigation, writing – review & editing. Guiting Chen: conceptualization, resources. Chuanbo Dai: resources, writing – review & editing, supervision.

Conflicts of interest

The authors declare no competing financial interest.

Acknowledgements

References

1 J. Wang and X. Zhan, *Acc. Chem. Res.*, 2021, **54**, 132–143.

2 F. Huang, Z. S. Bo, Y. H. Geng, X. H. Wang, L. X. Wang, Y. G. Ma, J. Hou, W. P. Hu, J. Pei, H. L. Dong, S. Wang, Z. Li, Z. G. Shuai, Y. F. Li and Y. Cao, *Acta Polym. Sin.*, 2019, **10**, 988–1046.

3 D. Wang, H. Liu, Y. Li, G. Zhou, L. Zhan, H. Zhu, X. Lu, H. Chen and C.-Z. Li, *Joule*, 2021, **5**, 945–957.

4 G. Zhang, F. R. Lin, F. Qi, T. Heumuller, A. Distler, H. J. Egelhaaf, N. Li, P. C. Y. Chow, C. J. Brabec, A. K. Jen and H. L. Yip, *Chem. Rev.*, 2022, **122**, 14180–14274.

5 Y. Cui, Y. Wang, J. Bergqvist, H. Yao, Y. Xu, B. Gao, C. Yang, S. Zhang, O. Inganäs, F. Gao and J. Hou, *Nat. Energy*, 2019, **4**, 768–775.

6 R. Sun, Y. Wu, X. Yang, Y. Gao, Z. Chen, K. Li, J. Qiao, T. Wang, J. Guo, C. Liu, X. Hao, H. Zhu and J. Min, *Adv. Mater.*, 2022, **34**, 2110147.

7 Q. Liu, Y. Jiang, K. Jin, J. Qin, J. Xu, W. Li, J. Xiong, J. Liu, Z. Xiao, K. Sun, S. Yang, X. Zhang and L. Ding, *Sci. Bull.*, 2020, **65**, 272–275.

8 X. Xu, W. Jing, H. Meng, Y. Guo, L. Yu, R. Li and Q. Peng, *Adv. Mater.*, 2023, **35**, 2208997.

9 Y. Wei, Z. Chen, G. Lu, N. Yu, C. Li, J. Gao, X. Gu, X. Hao, G. Lu, Z. Tang, J. Zhang, Z. Wei, X. Zhang and H. Huang, *Adv. Mater.*, 2022, **34**, 2204718.

10 P. Bi, J. Wang, Y. Cui, J. Zhang, T. Zhang, Z. Chen, J. Qiao, J. Dai, S. Zhang, X. Hao, Z. Wei and J. Hou, *Adv. Mater.*, 2023, **35**, e2210865.

11 L. Meng, H. Liang, G. Song, M. Li, Y. Huang, C. Jiang, K. Zhang, F. Huang, Z. Yao, C. Li, X. Wan and Y. Chen, *Sci. China: Chem.*, 2023, **66**, 808–815.

12 L. Zhu, M. Zhang, J. Xu, C. Li, J. Yan, G. Zhou, W. Zhong, T. Hao, J. Song, X. Xue, Z. Zhou, R. Zeng, H. Zhu, C. C. Chen, R. C. I. MacKenzie, Y. Zou, J. Nelson, Y. Zhang, Y. Sun and F. Liu, *Nat. Mater.*, 2022, **21**, 656–663.

13 S. Zhang, X. Ma, L. Niu, S. Y. Jeong, H. Y. Woo, Z. Zhou and F. Zhang, *Sol. RRL*, 2023, **7**, 2200957.

14 C. Zhu, K. Hu, L. Meng, X. Kong, W. Lai, S. Qin, B. Qiu, J. Zhang, Z. Zhang, Y. Wu, X. Li and Y. Li, *CCS Chem.*, 2023, DOI: 10.31635/ccschem.022.202202491.

15 C. Han, J. Wang, S. Zhang, L. Chen, F. Bi, J. Wang, C. Yang, P. Wang, Y. Li and X. Bao, *Adv. Mater.*, 2023, **35**, 2208986.

16 C. Li, J. Zhou, J. Song, J. Xu, H. Zhang, X. Zhang, J. Guo, L. Zhu, D. Wei, G. Han, J. Min, Y. Zhang, Z. Xie, Y. Yi, H. Yan, F. Gao, F. Liu and Y. Sun, *Nat. Energy*, 2021, **6**, 605–613.

17 M. D. Perez, C. Borek, S. R. Forrest and M. E. Thompson, *J. Am. Chem. Soc.*, 2009, **131**, 9281–9286.

18 H. Sun, T. Liu, J. Yu, T.-K. Lau, G. Zhang, Y. Zhang, M. Su, Y. Tang, R. Ma, B. Liu, J. Liang, K. Feng, X. Lu, X. Guo, F. Gao and H. Yan, *Energy Environ. Sci.*, 2019, **12**, 3328–3337.

19 P. Liu, K. Zhang, F. Liu, Y. Jin, S. Liu, T. P. Russell, H. L. Yip, F. Huang and Y. Cao, *Chem. Mater.*, 2014, **26**, 3009–3017.

20 T. Dai, A. Tang, Z. He, M. Du, P. Lei, Q. Zeng, Z. Wang, Y. Wang, S. Lu, Y. Zhong and E. Zhou, *Energy Environ. Sci.*, 2023, **16**, 2199–2211.

21 X. Yuan, Y. Zhao, T. Zhan, J. Oh, J. Zhou, J. Li, X. Wang, Z. Wang, S. Pang, P. Cai, C. Yang, Z. He, Z. Xie, C. Duan, F. Huang and Y. Cao, *Energy Environ. Sci.*, 2021, **14**, 5530–5540.

22 H. C. Chen, Y. H. Chen, C. C. Liu, Y. C. Chien, S. W. Chou and P. T. Chou, *Chem. Mater.*, 2012, **24**, 4766–4772.

23 Q. Fan, X. Xu, Y. Liu, W. Su, X. He, Y. Zhang, H. Tan, Y. Wang, Q. Peng and W. Zhu, *Polym. Chem.*, 2016, **7**, 1747–1755.

24 D. Dang, W. Chen, S. Himmelberger, Q. Tao, A. Lundin, R. Yang, W. Zhu, A. Salleo, C. Müller and E. Wang, *Adv. Energy Mater.*, 2014, **4**, 1400680.

25 Z. Zheng, O. M. Awartani, B. Gautam, D. Liu, Y. Qin, W. Li, A. Bataller, K. Gundogdu, H. Ade and J. Hou, *Adv. Mater.*, 2016, **29**, 1604241.

26 C. Sun, S. Qin, R. Wang, S. Chen, F. Pan, B. Qiu, Z. Shang, L. Meng, C. Zhang, M. Xiao, C. Yang and Y. Li, *J. Am. Chem. Soc.*, 2020, **142**, 1465–1474.

27 J. Yuan, L. Qiu, Z. G. Zhang, Y. Li, Y. Chen and Y. Zou, *Nano Energy*, 2016, **30**, 312–320.

28 S. Xu, L. Feng, J. Yuan, Z. G. Zhang, Y. Li, H. Peng and Y. Zou, *ACS Appl. Mater. Interfaces*, 2017, **9**, 18816–18825.

29 C. Zhu, L. Meng, J. Zhang, S. Qin, W. Lai, B. Qiu, J. Yuan, Y. Wan, W. Huang and Y. Li, *Adv. Mater.*, 2021, **33**, e2100474.

30 H. Yan, Z. Chen, Y. Zheng, C. Newman, J. R. Quinn, F. Dotz, M. Kastler and A. Facchetti, *Nature*, 2009, **457**, 679–686.

31 Z. Li, L. Ying, P. Zhu, W. Zhong, N. Li, F. Liu, F. Huang and Y. Cao, *Energy Environ. Sci.*, 2019, **12**, 157–163.

32 H. Li, F. S. Kim, G. Ren, E. C. Hollenbeck, S. Subramaniyan and S. A. Jenekhe, *Angew. Chem., Int. Ed.*, 2013, **52**, 5513–5517.

33 H. Li, F. S. Kim, G. Ren and S. A. Jenekhe, *J. Am. Chem. Soc.*, 2013, **135**, 14920–14923.

34 O. K. Kwon, J. H. Park, S. K. Park and S. Y. Park, *Adv. Energy Mater.*, 2015, **5**, 1400929.

35 G. Zhang, H. Ning, H. Chen, Q. Jiang, J. Jiang, P. Han, L. Dang, M. Xu, M. Shao, F. He and Q. Wu, *Joule*, 2021, **5**, 931–944.

36 H. Ning, Q. Jiang, P. Han, M. Lin, G. Zhang, J. Chen, H. Chen, S. Zeng, J. Gao, J. Liu, F. He and Q. Wu, *Energy Environ. Sci.*, 2021, **14**, 5919–5928.

37 K. Zhang, F. Huang and Y. Cao, *Acta Polym. Sin.*, 2017, **9**, 1400–1414.

38 Z. Hu, Y. Lei, F. Huang and Y. Cao, *Sci. China: Chem.*, 2017, **60**, 1–12.

39 J. L. Wu, F. C. Chen, Y. S. Hsiao, F. C. Chien, P. Chen, C. H. Kuo, M. H. Huang and C. S. Hsu, *ACS Nano*, 2011, **5**, 959–967.

40 B. He, Q. Yin, B. Xie, J. Zhang, R. Xie, Z. Hu, X. Peng, F. Huang and Y. Cao, *Polym. Chem.*, 2020, **11**, 1653–1662.

41 S. M. H. Rizvi and B. Mazhari, *J. Appl. Phys.*, 2017, **121**, 155501–155508.

42 M. M. Mandoc, F. B. Kooistra, J. C. Hummelen, B. D. Boer and P. W. M. Blom, *Appl. Phys. Lett.*, 2007, **91**, 263505.

43 D. Luo, L. Li, Y. Shi, J. Zhang, K. Wang, X. Guo and A. K. Kyaw, *J. Mater. Chem. A*, 2021, **9**, 14948–14957.

44 Z. Liu, Q. Mao, J. Wang, F. Wu, D. Zhou, Y. Cheng, S. Huang, B. Huang, C. Yang and L. Chen, *ChemSusChem*, 2022, **15**, e202102563.